Acta Scientific Pharmaceutical Sciences (ISSN: 2581-5423)

Volume 8 Issue 4 April 2024

Research Article

Theoretical Investigation on N-heterocyclic Carbene-Catalyzed Enantioselective [3 + 3] Annulation of Enal with 5-aminopyrazole for Construction of Pyrazolo[3,4-b]pyridone

Nan Lu*, Chengxia Miao and Xiaozheng Lan

College of Chemistry and Material Science, Shandong Agricultural University, Taian City, P.R. China

***Corresponding Author:** Nan Lu, College of Chemistry and Material Science, Shandong Agricultural University, Taian City, P.R. China.

DOI: 10.31080/ASPS.2024.08.1048

Received: February 26, 2024

Published: March 08, 2024

Abstract

The mechanism is investigated for [3 + 3] annulation of cinnamaldehyde with 5-aminopyrazole catalyzed by N-heterocyclic carbene (NHC) leading to pyrazolo[3,4-b]pyridone. The enal is attacked by NHC generating Breslow intermediate, the oxidation of which gives α,β-unsaturated acyazolium. After donating amino H, the 1,4-addition of 5-aminopyrazole is rate-limiting step. The enantioselectivity is determined by the attack to less hindered face of NHC-enal complex. Once NHC is departed, the intramolecular lactamization readily occurs followed by tautomerization. The product with favored s isomer is cooperatively controlled both by thermodynamics and kinetics with recovered NHC catalyst. Although the 1,4-addition reaction path is reasonable and more easily, the 1,2-addition followed by an intramolecular Claisen rearrangement reaction path is also possible. The positive solvation effect is suggested by decreased absolute and activation energies in THF solution compared with in gas.

Keywords: [3 + 3] Annulation; Enantioselective; N-heterocyclic Carbene; 5-aminopyrazole; Enal

Introduction

As interesting heteroatom-rich and fused bicyclic structures, pyrazolo[3,4-b]-pyridones have been extensively explored in new drug discovery as agrochemicals and pharmaceuticals owing to varied biological activities [1-3]. For instance, pyrano[2,3-d]pyridine and pyrazolo[3,4-b]pyridine derivatives were synthesized by microwave irradiation. The insecticidal activity of compound containing pyrazolo[3,4-b]pyridone fragment was proved to be excellent against Sitophilus oryzae [4]. A derivative spiropyrazolopyridone was potential dengue virus inhibitors showing exceptional antiviral activity [5]. Novel pyrazolo[3,4-b]pyridinone was obtained by "On-water" facile method exhibiting anti-influenza virus activity especially on H5N1 pseudovirus [6]. Fragment-based discovery of pyrazolopyridone was employed as JAK1 kinase inhibitor with high selectivity [7]. Recently, a series of chiral pyrazolo[3,4-b]pyridine derivatives were designed for antifungal investigation against Phytophthora capsici or for pepper protection [8-10]. Therefore, the strategies of enantioselective construction of pyrazolo[3,4-b] pyridones is in high demand considering the increasing application in pharmaceutical science. The development of efficient and green methods constructing such molecular skeleton is urgently needed and has attracted considerable attention.

As versatile Lewis-base organocatalyst, N-heterocyclic carbene (NHC) can facilitate various asymmetric carbon–carbon and carbon–heteroatom construction [11]. Ye synthesized a series of bifunctional NHCs derived from L-pyroglutamic acid improving stereochemical control through synchronous activation of both reaction partners [12]. Wang achieved asymmetric synthesis of axially chiral scaffolds by using NHCs [13]. Du discovered alkynyl acylazolium as 1,3-bielectrophilic 3C-synthon in NHC-organocatalysis [14]. To construct complex molecules with enantiopure structure, α,β-unsaturated acylazolium was intensively employed in many annulation strategies as key intermediate. The enantioselective functionalization of 3-aminobenzofuran was realized using 2-bromoenal as coupling partner at C2-position. Via oxidative NHC catal-

ysis, triaryl-2-pyrone was enantioselectively obtained with monoaxial or contiguous diaxes. Ni/NHC cooperative catalysis enabled asymmetric redox allylic alkylation to access 3,3'-disubstituted oxindole. 4-aryl α-carboline skeleton was constructed through atroposelective formal [3 + 3] annulation of 4-nitrophenyl 3-arylpropiolate with 2-sulfonamidoindoline [15-19]. 5-aminopyrazole is popular binucleophile in construction of functional compounds, such as C(sp2)-H thiocyanation of aminopyrazoles, amino uracils, and enamines mediated by hydrogen peroxide, visible light-mediated C(sp2)−H selenylation of amino pyrazole and Cu(II)-catalyzed synthesis of substituted pyrazolo[1,5-a]pyrimidines via [3 + 3] annulation of saturated ketones with aminopyrazoles [20-22].

Recently, many new strategies were developed with efficient asymmetric synthetic route promoted by NHC. Chi described chiral NHC-catalyzed [3 + 3] cycloaddition for synthesis of pyrazolo[3,4-b]pyridones with excellent yield and optical purity. Wang also reported similar enantioselective method constructing a structurally diverse set of high value dihydropyrazolo[3,4-b]pyridine-6-ones from α-bromoenals with 5-aminopyrazoles [23,24]. In the field of new drug design and natural product synthesis with pyrazolo[3,4-b]pyridines structural core, a breakthrough was Duan's enantioselective [3 + 3] annulation of enal with 5-aminopyrazole catalyzed by NHC [25]. Although pyrazolo[3,4-b]pyridine was provided, there is no report about detailed mechanistic study explaining the excellent enantioselectivity. What's the function of NHC in nucleophilic addition with enal generating Breslow intermediate? How to distinguish the superiority between 1,4 addition and 1,2-addition of 5-aminopyrazole to α,β-unsaturated acyazolium intermediate? Whether the enantioselectivity is influenced by the following reaction details after 1,4 addition or 1,2-addition? To solve these mechanic problems in experiment, an in-depth theoretical study was necessary for this enantioselective [3 + 3] annulation. The density functional theory (DFT) method was employed focusing on the promotion of NHC during the dominance of enantiopure products.

Methods

Optimized structures were obtained at M06-2X/6-31G(d) level of theory with GAUSSIAN09 [26]. In tests of popular DFT methods [27], M06-2X functional attained smaller standard deviation of difference between calculated value and experimental value in geometries than B3LYP including Becke's three-parameter hybrid functional combined with Lee−Yang−Parr correction for correlation [28,29]. The best compromise between accuracy and time consumption was provided with 6-31G(d) basis set on energy calculations. Also, M06-2X functional was found to give relatively accurate results for catalysed enantioselective (4 + 3), concerted [4 + 2], stepwise (2 + 2) cycloaddition and catalysed Diels–Alder reactions [30,31]. Together with the best performance on noncovalent interaction, M06-2X functional is believed to be suitable for this system [32-34]. The nature of each structure was verified by performing harmonic vibrational frequency calculations. Intrinsic reaction coordinate (IRC) calculations were examined to confirm the right connections among key transition-states and corresponding reactants and products. Harmonic frequency calculations were carried out at the M06-2X/6-31G(d) level to gain zero-point vibrational energy (ZPVE) and thermodynamic corrections at 298.15 K and 1 atm for each structure in TetraHydroFuran (THF).

The solvation-corrected free energies were obtained at the M06-2X/6-311++G(d,p) level by using integral equation formalism polarizable continuum model (IEFPCM) in Truhlar's "density" solvation model [35-39] on the M06-2X/6-31G(d)-optimized geometries. As an efficient method obtaining bond and lone pair of a molecule from modern ab initio wave functions, NBO procedure was performed with Natural bond orbital (NBO3.1) to characterize electronic properties and bonding orbital interactions [40-42]. The wave function analysis was provided using Multiwfn_3.7_dev package [43].

Results and Discussion

Based on previous research [21-25], the mechanism was explored for [3 + 3] annulation of cinnamaldehyde 1 with 5-aminopyrazole 2 catalyzed by NHC model leading to pyrazolo[3,4-b] pyridone 3 (Scheme 1). Depicted by the black arrow of Scheme 2, the enal 1 was attacked by nucleophilic NHC generating Breslow intermediate I, the oxidation of which gives α,β-unsaturated acyazolium structure II. After donating amino H, as is illustrated by the red arrow, the 1,4-addition of 2 proceeds from two sides of planar II affords intermediate III, wherein the enantioselectivity is influenced by the different hindered face (path A). Once NHC is departed, the intramolecular lactamization readily occur giving intermediate V followed with tautomerization induced by proton transfer. Alternatively, the 1,2-addition of 2 is plausible shown by blue arrow (path B) producing III-1, from which V can also be yielded

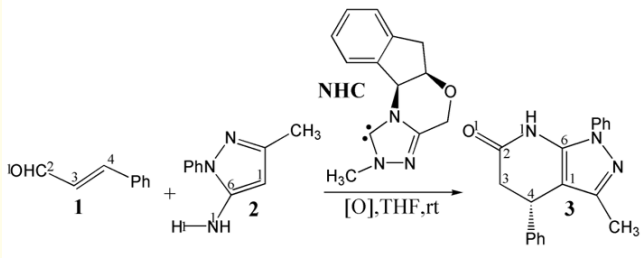

Scheme 1: N-heterocyclic carbene-catalyzed [3 + 3] annulation of cinnamaldehyde 1 with 5-aminopyrazole 2 leading to pyrazolo[3,4-b]pyridone 3.

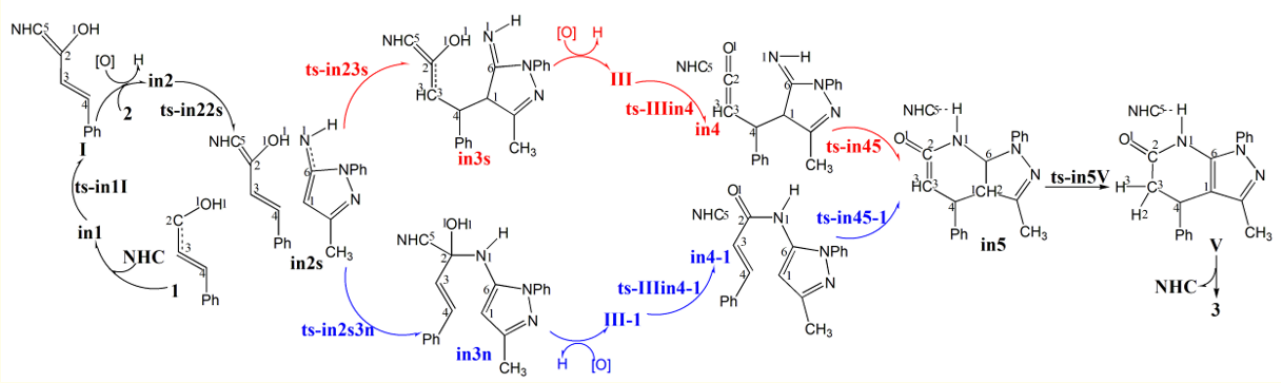

Scheme 2: Proposed reaction mechanism of N-heterocyclic carbene-catalyzed [3 + 3] annulation of 5-aminopyrazole 2 with cinnamaldehyde 1 leading to pyrazolo[3,4-b]pyridone 3. TS is named according to the two intermediates it connects.

after releasing NHC, cyclization/tautomerization. The product 3 is finally obtained via proton transfer with recovered NHC catalyst. The optimized structures of TSs in Scheme 2 were listed by Figure 1. The activation energy was shown in Table 1 for all steps. Supplementary Table S1, Table S2 provided the relative energies of all stationary points. According to experiment, the Gibbs free energies in THF solution phase are discussed here.

Breslow intermediate generation

With reactive enal 1 in hand, the complex in1 between it and NHC was taken as starting point, from which the nucleophilic addition of NHC proceeds via ts-in1I as step 1 with a activation energy of 12.4 kcal mol^{-1} exothermic by -45.6 kcal mol^{-1} furnishing Breslow intermediate I. This step is fairly easy whether from small barrier kinetically or from large heat release thermodynamically. The transition vector includes the link of C2 to C5 until contracted to C2-C5 double bond and elongation of C2-O1, C2-C3 (2.43, 1.32, 1.48 Å) (Figure S1a). Thus I is rather stable with conjugated C2-C5 and C3-C4 diene structure.

Once the oxidation of I happens, previous hydroxyl turns to be carbonyl group in the resultant α,β-unsaturated acyazolium structure II, which is thereby easy to accept proton from amino of 2. Via ts-in22s, the activation energy of step 2 is 7.1 kcal mol^{-1} with respect to in2, the complex binding 2 and II taken as starting point for following two steps. A reactive intermediate in2s is generated endoergic by 6.3 kcal mol^{-1} involving depronated 2 more nucleophilic and recovered I. The transition vector of ts-in22s corresponds to H1 transfer from N1 to O1 (1.33, 1.16 Å) (Figure S1b).

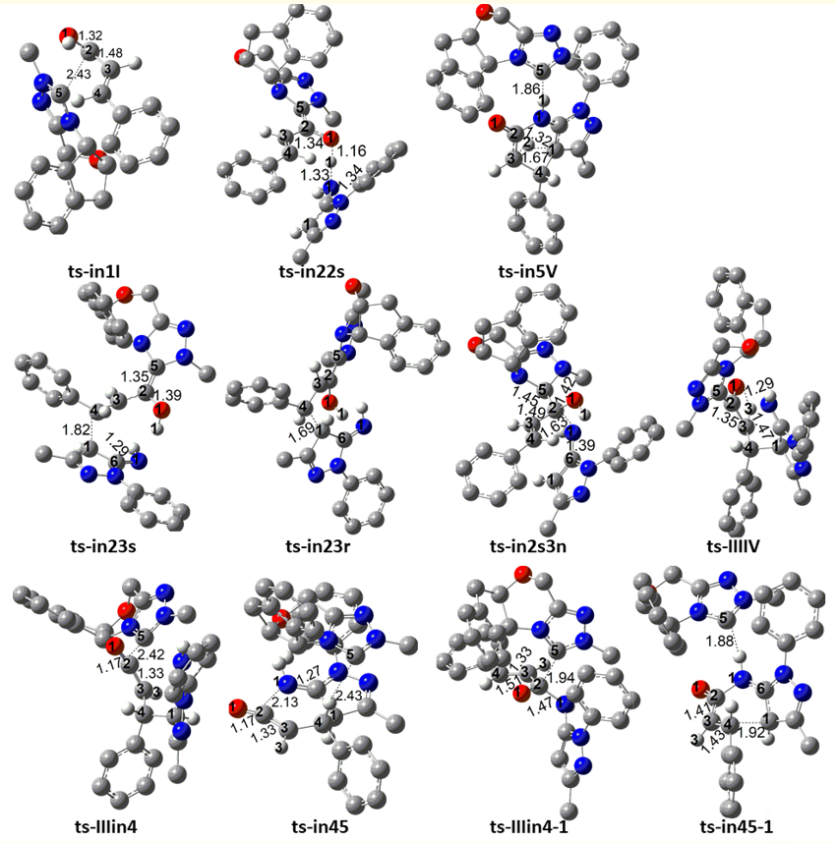

Figure 1: Geometric structures of TSs for enantioselective [3 + 3] annulation of 2 with 1 leading to 3. Selected bond distances are given in Å. Irrelevant hydrogen atoms are omitted for clarity.

Table 1: The activation energy (in kJ mol^{-1}) of all reactions in gas and solvent.

TS	$\Delta G^{\neq}_{gas}$	$\Delta G^{\neq}_{sol}$
ts-in1I	13.6	12.4
ts-in22s	3.7	7.1
ts-in23s	33.3	25.0
ts-in2s3n	56.2	54.3
ts-in23r	38.2	28.8
ts-IIIin4	20.8	28.9
ts-in45	2.1	1.5
ts-IIIin4-1	2.8	4.8
ts-in45-1	45.2	29.5
ts-in5V	21.0	12.9
ts-IIIIV	57.3	62.4

Table S1: Calculated relative energies (all in kcal mol^{-1}, relative to isolated species) for the ZPE-corrected Gibbs free energies (ΔG_{gas}), Gibbs free energies for all species in solution phase (ΔG_{sol}) at 298 K by M06-2X/6-311++G(d,p)//M06-2X/6-31G(d) method and difference between absolute energy.

Species	ΔG_{gas}	$\Delta G_{sol(THF)}$	$\Delta\Delta G_{sol-gas}$
1+nhc			
in1	0.00	0.00	-39.00
ts-in1I	13.60	12.39	-40.22
I	-47.85	-45.61	-36.76
1+2+nhc-h			
in2	0.00	0.00	-76.61
ts-in22s	3.73	7.10	-73.24
in2s	3.41	6.34	-73.68
ts-in23s	36.68	31.33	-81.96
ts-in2s3n	59.63	60.62	-75.63
in3s	34.39	26.91	-84.09
in3n	54.92	53.70	-77.84
in2r	3.19	3.72	-76.08
ts-in23r	41.44	32.55	-85.50
in3r	42.57	33.91	-85.28
1+2+nhc-2h			
III	0.00	0.00	-65.49
ts-IIIin4	20.79	28.88	-57.41
III-1	-2.14	13.46	-49.89
ts-IIIin4-1	0.61	18.27	-47.83
in4	8.15	22.07	-51.57
ts-in45	10.24	23.55	-52.18
in4-1	-25.47	-0.52	-40.55
ts-in45-1	19.68	29.01	-56.16
in5	6.31	13.50	-58.30
ts-in5V	27.29	26.45	-66.33
V	-40.68	-21.54	-46.35
ts-IIIIV	57.30	62.37	-60.42
IV	31.73	45.18	-52.04
1+2-2h			
3s	0.00	0.00	-29.76
3r	1.21	0.74	-30.23

Table S2: The activation energy (local barrier) (in kcal mol^{-1}) of all reactions in the gas, solution phase calculated with M06-2X/6-311++G(d,p)//M06-2X/6-31G(d) method and difference between the two.

TS	$\Delta G^{\neq}_{gas}$	$\Delta G^{\neq}_{sol}$	$\Delta\Delta G_{sol-gas}$
ts-in1I	13.6	12.4	-1.2
ts-in22s	3.7	7.1	3.4
ts-in23s	33.3	25.0	-8.3
ts-in2s3n	56.2	54.3	-1.9
ts-in23r	38.2	28.8	-9.4
ts-IIIin4	20.8	28.9	8.1
ts-in45	2.1	1.5	-0.6
ts-IIIin4-1	2.8	4.8	2.1
ts-in45-1	45.2	29.5	-15.6
ts-in5V	21.0	12.9	-8.0
ts-IIIIV	57.3	62.4	5.1

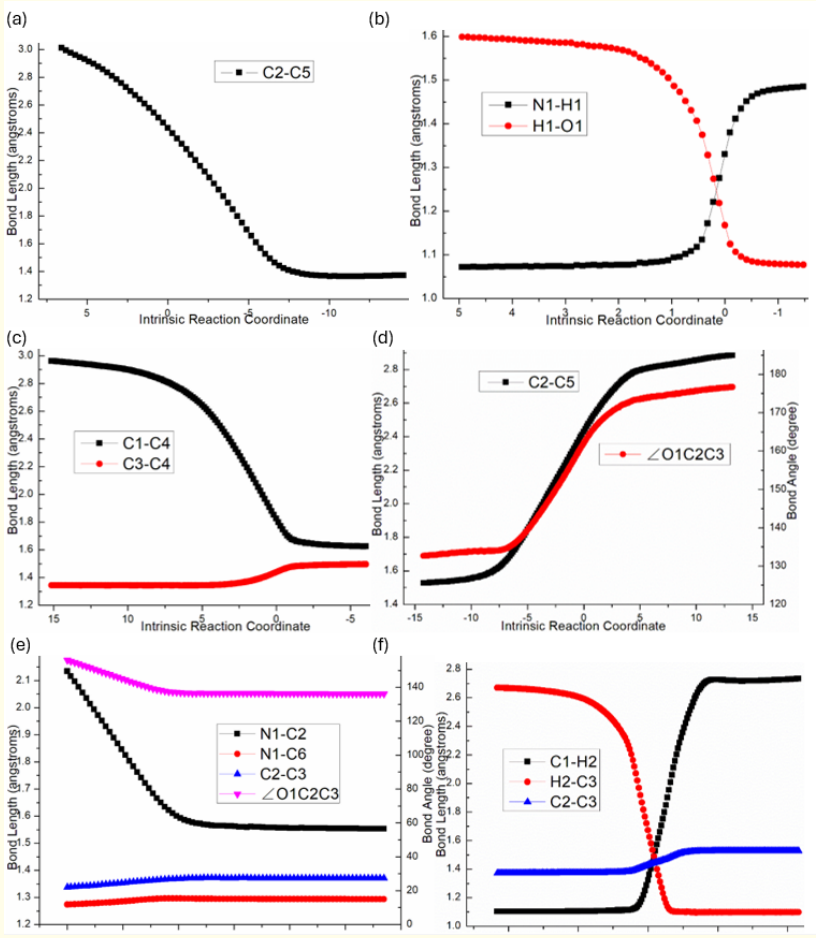

Figure 1: Evolution of bond lengths along the IRC for (a) ts-in1I (b) ts-in22s (c) ts-in23s (d) ts-IIIin4 (e) ts-in45 (f) ts-in5V at the M06-2X/6-311++G(d,p) level.

1,4-addition, NHC departure, intramolecular lactamization

There are two paths denoting nucleophilic 1,4- and 1,2-addition initiated from 2. Path A is the attack of negative C1 to C4 from less hindered face of I via ts-in23s as step 3 with a mediate barrier of 25.0 kcal mol^{-1} endoergic by 25.6 kcal mol^{-1} delivering reactive complex in3s (red dash line of Figure 2). Besides evident bonding of C1···C4, the transition vector consists of C3−C4 stretching from double to single (1.82, 1.40 Å) (Figure S1c). No change is observed for other atoms including the strong linkage with NHC.

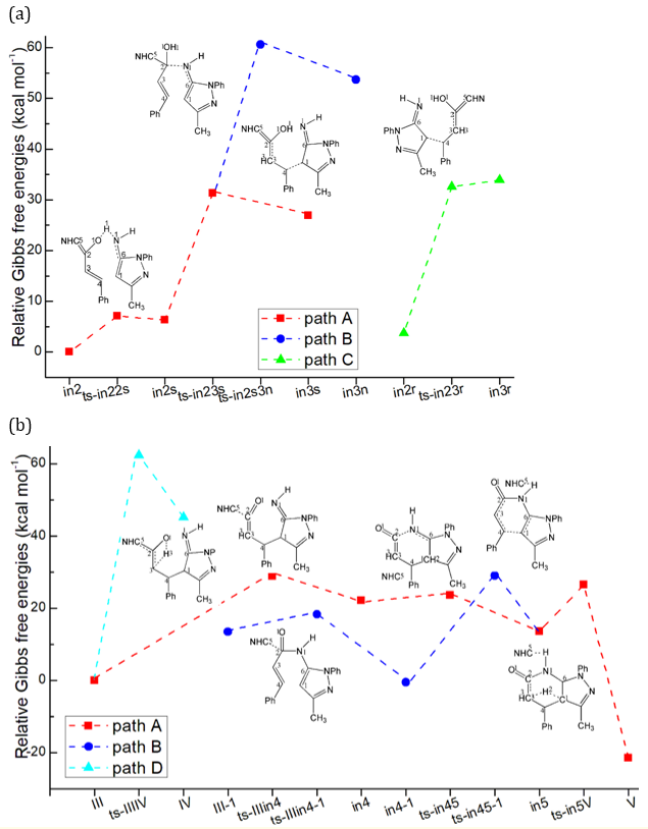

Figure 2: Relative Gibbs free energy profile of enantioselective [3 + 3] annulation of 2 with 1 in solvent phase starting from complex (a) in2 (b) III.(e) ts-in45 (f) ts-in5V at the M06-2X/6-311++G(d,p) level.

Between this step and the next one, hydroxyl of in3s becomes carbonyl group via a second oxidation leading to III as the starting point of step 4. That is NHC departure via ts-IIIin4 with activation energy of 28.9 kcal mol^{-1} relative to III affording in4 endoergic by 22.1 kcal mol^{-1}. The transition vector of ts-IIIin4 corresponds to the breaking down of C2-C5 bond, enlarge of O1-C2-C3 angle to 180° while still maintaining of C2-O1 and C2-C3 double bonds (2.42, 1.19, 1.33 Å) (Figure S1d). This suggests the cumulative diene structure of in4, in which although NHC is departed, weak C4-H···C5 H bond (2.43 Å) still exists between lone pair located on C5 and the precursor of product, which indicates the stabilization of NHC catalyst.

Thankfully under the preparation of former steps, the intramolecular lactamization in step 5 is fairly easy via ts-in45 with rather small of activation energy of 1.5 kcal mol^{-1} exothermic by -8.6 kcal mol^{-1} giving stable six-membered cyclic intermediate in5. The nucleophilic attack from negative N1 of imine to the middle positive C2 of cumulative diene can be described by transition vector of ts-in45 (2.13 Å) (Figure S1e). Kinetically, the NHC departure of step 4 is determined to be rate-limiting of path A.

1,2-addition, NHC departure, cyclization

Alternatively after giving amino H, the 1,2-addition of nucleophilic 2 may also occur denoted as path B, which is the attack of negative N1 to C2 via ts-in2s3n in step 3 (blue dash line of Figure 2) yielding reactive complex in3n. The transition vector demonstrates closing of imine N1 of 2 to sp3 C2 of II (1.63 Å) involving C2−O1, C2−C3, C2−C5 three single bonds (1.42, 1.49, 1.45 Å). Considering the high barrier of 54.3 kcal mol^{-1} and greatly endoergic by 47.4 kcal mol^{-1}, this 1,2-addition is not favorable compared with 1,4-addition for step 3. Next, hydroxyl of in3n is also oxidized to carbonyl group of III-1 as starting point of the following step 4 and step 5. Via ts-IIIin4-1, the activation energy of NHC departure is small to be only 4.8 kcal mol^{-1} owing to the carbonyl C2 in stable sp2 hybridization in contrast with unstable cumulative diene middle C2 in ts-IIIin4. Furthermore, the same reason makes resultant in4-1 also much lower in energy than counterpart in4 and exothermic by -14.0 kcal mol^{-1}. The transition vector of ts-IIIin4-1 corresponds to the cleavage of C5 from C2, where C2-N1 and C2-C3 are single bonds (1.94, 1.47, 1.51 Å). The step 5 is cycle-closing process via nucleophilic addition of C1 to C4 known as aza-Claisen rearrangement producing the same six-membered cyclic complex in5. The activation energy is somewhat increased to be 29.5 kcal mol^{-1} via ts-in45-1 endoergic by 14.0 kcal mol^{-1} to complete this step. The transition vector of ts-in45-1 is about nucleophilic attack of C1 to

C4, where C2-C3-C4 is represented as conjugated small π bond (1.92, 1.41, 1.43 Å) together with strong N1-H⋯C5 H bond (1.88 Å) contributed by NHC catalyst stabilizing its structure.

As precursor of the last complex V, the tautomerization of in5 is required via ts-in5V with a barrier of 12.9 kcal mol^{-1}exothermic by -35.0 kcal mol^{-1} substantially. The transition vector of ts-in5V corresponds to the proton transfer from C1 to C3 (1.32, 1.67 Å) (Figure S1f). Once the proton is received by C3, cumulative diene is replaced by stable sp2 hybrid C1 and C2. Evidently, this step is not only fairly easy itself but effectively pull the entire reaction. In addition, the enol isomer of III proposed by experiment is considered here denoted as IV, which can be achieved by proton shifting from C3 to O1 via ts-IIIIV through path D (cyan dash line of Figure 2b).

Enantioselectivity and solvent effect

Although excellent enantioselectivity of product **3** is obtained in experiment, whether it is determined by thermodynamic stability of enantiomers or is kinetically influenced by nucleophilic 1,4-addition namely C1⋯C4 bonding of preferred path A? Therefore the enantiomeric excess value (ee) of 3 is predicted using two methods applying difference between relative energy of isomers and activation energy of TSs. 3r is higher in energy by 0.74 kcal mol^{-1} than 3s. From path C (green dash line of Figure 2a), the barrier of ts-in23r is higher by 3.8 kcal mol^{-1} than that of ts-in23s. Here, based on the calculation of rate constant (k) in transition state theory, the calculated ee value of 3s is bigger than 95% in accordance with experiment. Hence the enantioselectivity of favored s isomer is cooperatively controlled by thermodynamics and kinetics.

The impact of THF solution is studied in view of the solvent effect on reaction estimated by our approach [32-34]. Obviously, the absolute energies of all stationary points in solution are lower than those in gas phase (Table S1). It is noticed that more oxidation reliefs the influence of solvent on annulation via both paths with relative energies decreased by -70∼-90 kcal mol^{-1} (once oxidation) vs -40∼-70 kcal mol^{-1} (twice). For most steps, the activation energies are reduced in solution phase compared with in gas (Table S2). Accordingly, the THF solution produces favorable influence on this [3 + 3] annulation of cinnamaldehyde with 5-aminopyrazole catalyzed by N-heterocyclic carbene leading to pyrazolo[3,4-b] pyridone.

Conclusion

Our DFT calculations provide the first theoretical investigation on [3 + 3] annulation of cinnamaldehyde with 5-aminopyrazole catalyzed by N-heterocyclic carbene leading to pyrazolo[3,4-b] pyridone. The enal was attacked by nucleophilic NHC generating Breslow intermediate, the oxidation of which gives α,β-unsaturated acyazolium structure. After donating amino H, the 1,4-addition of 5-aminopyrazole from two different hindered face influences the enantioselectivity. Once NHC is departed, the intramolecular lactamization readily occurs followed by tautomerization. The nucleophilic 1,4-addition is rate-limiting step. The product is obtained with recovered NHC catalyst. Although the 1,4-addition reaction path is reasonable and more easily, the 1,2-addition followed by an intramolecular Claisen rearrangement reaction path is also possible and cannot be completely ruled out.

Based on the comparison between possible paths, the enantioselectivity of product is determined by 1,4-addition of 5-aminopyrazole to the less hindered face of NHC catalyst-enal complex. The favored s isomer is cooperatively controlled by thermodynamics and kinetics. The positive solvation effect is suggested by decreased absolute and activation energies in THF solution compared with in gas.

Acknowledgements

This work was supported by National Natural Science Foundation of China (21973056, 21972079) and Natural Science Foundation of Shandong Province (ZR2019MB050).

Bibliography

1. Dorostkar-Ahmadi N., *et al.* "Facile synthesis of new 6-alkylamino-1H-pyrazolo[3,4-b]pyridine-5-carbonitrile derivatives". *Journal of Heterocyclic Chemistry* 55.11 (2018): 2635-2639.

2. Lichitsky BV., *et al.* "Benzimidazolyl-pyrazolo[3,4-b]pyridinones, Selective Inhibitors of MOLT-4 Leukemia Cell Growth and Sea Urchin Embryo Spiculogenesis: Target Quest". *ACS Combinatorial Science* 21 (2019): 805-816.

3. Kim HS., *et al.* "Discovery of novel pyrazolo-pyridone DCN1 inhibitors controlling cullin neddylation". *Journal of Medicinal Chemistry* 62 (2019): 8429-8442.

4. Chaudhari SA., *et al.* "Synthesis of pyrano[2,3-d]pyridine, pyrazolo[3,4-b]pyridine derivatives by microwave irradiation and study of their insecticidal activity". *Journal of Chemical and Pharmaceutical Research* 7 (2015): 476.

5. Zou B., *et al.* "Lead optimization of spiropyrazolopyridones: a new and potent class of dengue virus inhibitors". *ACS Medicinal Chemistry Letters* 6 (2015): 344-348.

6. Zeng LY., *et al.* ""On-water" facile synthesis of novel pyrazolo[3,4-b]pyridinones possessing anti-influenza virus activity". *ACS Combinatorial Science* 19 (2017): 437-446.

7. Hansen BB., *et al.* "Fragment-based discovery of pyrazolopyridones as JAK1 inhibitors with excellent subtype selectivity". *Journal of Medicinal Chemistry* 63 (2020): 7008-7032.

8. Jin JH., *et al.* "A New ethylene-responsive factor CaPTI1 gene of pepper (Capsicum annuum L.) involved in the regulation of defense response to Phytophthora capsici". *Frontiers in Plant Science* 6 (2016): 1217.

9. Wang Z., *et al.* "Protocol of Phytophthora capsici transformation using the CRISPR-Cas9 system". *Methods Mol. Biol.* 1848 (2018): 265-274.

10. Evallo E., *et al.* "Colletotrichum fructicola associated with fruit anthracnose of persimmon". *Journal of Phytopathology* 170.3 (2022): 194-201.

11. Hopkinson MN., *et al.* "An overview of N-heterocyclic carbenes". *Nature* 510 (2014): 485-496.

12. Chen XY., *et al.* "Bifunctional N-Heterocyclic Carbenes Derived from l-Pyroglutamic Acid and Their Applications in Enantioselective Organocatalysis". *Accounts of Chemical Research* 53 (2020): 690-702.

13. Wang J., *et al.* "Recent Progress toward the Construction of Axially Chiral Molecules Catalyzed by an N-heterocyclic Carbene". *ACS Catalyst* 11 (2021): 12520-12531.

14. Gao J., *et al.* "Alkynyl Acylazolium: a Versatile 1,3-Bielectrophilic 3C-Synthonin NHC-Organocatalysis". *Chemical Record* 23.7 (2023): e202300046.

15. Barik S., *et al.* "Kinetic Resolution Approach to the Synthesis of C–N Axially Chiral N-Aryl Aminomaleimides via NHC-Catalyzed [3 + 3] Annulation". *Organic Letter* 24 (2022): 5456-5461.

16. Barik S., *et al.* "Catalytic, Enantioselective C2-Functionalization of 3-Aminobenzofurans Using N-Heterocyclic Carbenes". *Organic Letter* 22 (2020): 3865-3869.

17. Zhang SC., *et al.* "Enantioselective Access to Triaryl-2-pyrones with Monoaxial or Contiguous C–C Diaxes via Oxidative NHC Catalysis". *ACS Catalyst* 13 (2023): 2565-2575.

18. Fan T., *et al.* "Asymmetric Redox Allylic Alkylation to Access 3,3′-Disubstituted Oxindoles Enabled by Ni/NHC Cooperative Catalysis". *Angewandte Chemie* 61.22 (2022): e202201678.

19. Ma R., *et al.* "Atroposelective Synthesis of Axially Chiral 4-Aryl α-Carbolines via N-Heterocyclic Carbene Catalysis". *Organic Letter* 23 (2021): 4267-4272.

20. Ali D., *et al.* "Hydrogen Peroxide-Mediated Rapid Room Temperature Metal-Free C (sp 2)-H Thiocyanation of Amino Pyrazoles, Amino Uracils, and Enamines". *The Journal of Organic Chemistry* 85 (2020): 13610-13620.

21. Ali D., *et al.* "Visible Light-Mediated C (sp 2)–H Selenylation of Amino Pyrazole and Amino Uracils in the Presence of Rose Bengal as an Organophotocatalyst". *The Journal of Organic Chemistry* 87 (2022): 1230-1239.

22. Ren J., *et al.* "An Approach for the Synthesis of Pyrazolo[1,5-a] pyrimidines via Cu (II)-Catalyzed [3 + 3] Annulation of Saturated Ketones with Aminopyrazoles". *The Journal of Organic Chemistry* 86 (2021): 12762-12771.

23. Nie G., *et al.* "Enantioselective Synthesis of Pyrazolo[3,4-b]pyridone Derivatives with Antifungal Activities against Phytophthora capsici and Colletotrichum fructicola". *Organic Letter* 25 (2023): 134-139.

24. Li Y., *et al.* "Enantioselective Synthesis of Dihydropyrazolo[3,4-b]pyridin-6-ones via N-Hetero-cyclic Carbene Catalyzed [3 + 3] Cycloaddition of α-Bromoenals with 5-Aminopyrazoles". *Advanced Synthesis and Catalysis* 365 (2023): 490-495.

25. Li J., *et al.* "N-Heterocyclic Carbene-Catalyzed [3 + 3] Annulation of 5-Aminopyrazoles with Enals: Enantioselective Synthesis of Pyrazolo[3,4-b]pyridines". *The Journal of Organic Chemistry* 88 (2023): 16621-16632.

26. Frisch MJ., *et al.* Gaussian 09, Revision B.01, Gaussian, Inc, Wallingford, CT (2009).

27. Hay PJ., *et al.* "Ab initio effective core potentials for molecular calculations-potentials for the transition-metal atoms Sc to Hg". *The Journal of Chemical Physics* 82.1 (1985): 270-283.

28. Becke AD. "Density-functional thermochemistry. IV. A new dynamical correlation functional and implications for exact-exchange mixing". *The Journal of Chemical Physics* 104.3 (1996): 1040-1046.

29. Lee CT., *et al.* "Development of the Colle-Salvetti correlation-energy formula into a functional of the electron density". *Physical Review B* 37.2 (1988): 785-789.

30. Li X., *et al.* "Bifunctional Thiourea-Catalyzed Asymmetric Inverse-Electron-Demand Diels-Alder Reaction of Allyl Ketones and Vinyl 1,2-Diketones via Dienolate Intermediate". *Organic Letter* 21.7 (2019): 1979-1983.

31. Krenske E H., *et al.* "Computational Analysis of the Stereochemical Outcome in the Imidazolidinone-Catalyzed Enantioselective (4 + 3)-Cycloaddition Reaction". *The Journal of Organic Chemistry* 80.2 (2015): 744-750.

32. Lv H., *et al.* "Ionic Liquid Catalyzed C-C Bond Formation for the Synthesis of Polysubstituted Olefins". *European Journal of Organic Chemistry* 2022.45 (2022): e202201222.

33. Zhuang H., *et al.* "Bu4NHSO4-Catalyzed Direct N-Allylation of Pyrazole and its Derivatives with Allylic Alcohols in Water: A Metal-free, Recyclable and Sustainable System". *Advanced Synthesis and Catalysis* 363.24 (2021): 5461-5472.

34. Lu, N., *et al.* "Theoretical investigation on the mechanism and enantioselectivity of organocatalytic asymmetric Povarov reactions of anilines and aldehydes". *International Journal of Quantum Chemistry* 120 (2020): e26574.

35. Tapia O. "Solvent effect theories: Quantum and classical formalisms and their applications in chemistry and biochemistry". *Journal of Mathematical Chemistry* 10.1 (1992): 139-181.

36. Tomasi J., *et al.* "Molecular Interactions in Solution: An Overview of Methods Based on Continuous Distributions of the Solvent". *Chemical Review* 94.7 (1994): 2027-2094.

37. Simkin BY., *et al.* "Quantum Chemical and Statistical Theory of Solutions—A Computational Approach". Ellis Horwood, London (1995).

38. Tomasi J., *et al.* "Quantum Mechanical Continuum Solvation Models". *Chemical Review* 105.8 (2005): 2999-3093.

39. Marenich AV., *et al.* "Universal slovation model based on solute electron density and on a continuum model of the solvent defined by the bulk dielectric constant and atomic surface tensions". *The Journal of Physical Chemistry B* 113.18 (2009): 6378-6396.

40. Reed AE., *et al.* "Natural population analysis". *The Journal of Chemical Physics* 83.2 (1985): 735-746.

41. Reed AE., *et al.* "Intermolecular interactions from a natural bond orbital donor-acceptor view point". *Chemical Review* 88.6 (1988): 899-926.

42. Foresman, JB., *et al.* "Exploring Chemistry with Electronic Structure Methods". 2nd ed., Gaussian, Inc., Pittsburgh (1996).

43. Lu T., *et al.* "Multiwfn: A multifunctional wavefunction analyzer". *Journal of Computational Chemistry* 33.5 (2012): 580-592.